Loading of Cisplatin into Mesoporous Silica Nanoparticles: Effect of Surface Functionalization

Mathieu Varache, Igor Bezverkhyy, Guy Weber, Lucien Saviot, Remi Chassagnon, Florence Baras, Frédéric Bouyer

Interface Components: Nanoparticles, Colloids, Emulsions, Surfactants, Proteins, Polymers

Loading of Cisplatin into Mesoporous Silica Nanoparticles: Effect of Surface Functionalization

Mathieu Varache, Igor Bezverkhyy, Guy Weber, Lucien Saviot, Remi Chassagnon, Florence Baras, and Frédéric Bouyer

Langmuir, **Just Accepted Manuscript** • DOI: 10.1021/acs.langmuir.9b00954 • Publication Date (Web): 06 Jun 2019

Loading of Cisplatin into Mesoporous Silica Nanoparticles: Effect of Surface Functionalization

Mathieu Varache[†], Igor Bezverkhyy[†], Guy Weber[†], Lucien Saviot[†], Rémi Chassagnon[†], Florence Baras[†] and Frédéric Bouyer[†,*]

[†]*Laboratoire Interdisciplinaire Carnot de Bourgogne, UMR 6303 CNRS-Université Bourgogne Franche-Comté, 9 Avenue Alain Savary, BP 47 870, F-21078 DIJON Cedex, France*

[*]Corresponding author (email: frederic.bouyer@u-bourgogne.fr)

Abstract

Cisplatin (CDDP) plays a crucial role in the treatment of various malignant tumors. However, its clinical efficacy and applicability are restricted by issues of toxicity and resistance. Here, for drug delivery purposes, the outer surface of MCM-41 silica nanoparticles (MSNs) were functionalized with polyethylene glycol (PEG, M_w = 10,000 g/mol) or low molecular weight (M_w = 1,800 g/mol) branched polyethyleneimine (PEI). Given the strong affinity of sulfur for platinum, thiol-functionalized MSNs were synthesized for comparison by co-condensation with (3-mercaptopropyl)triethoxysilane (MPTES). CDDP loading was performed either by adsorption or impregnation in aqueous media without the use of dimethylsulfoxide (DMSO) as a solubilizer. CDDP loading capacities obtained by impregnation were higher than those obtained by adsorption and varied from 3.9 to 16.1 wt%, depending on the functional group. Loaded nanomaterials were characterized by SEM, STEM-HAADF and Raman spectroscopy. Depending upon the functional groups, platinum-based species were either dispersed in the nanomaterials as nanocrystals or uniformly distributed as molecular species. The spectral signature of CDDP was strongly modified when platinum species were homogeneously distributed within the nanomaterials. Preliminary drug release studies performed at 37°C showed that the behavior of the CDDP loaded MSNs strongly depends on the nature of the present functional groups. Among the functionalization routes investigated in this paper, PEI-based functionalization showed the most promising results for further applications in controlled drug release with an absence of burst release and a sustained release over 72 h.

Keywords: mesoporous silica nanomaterials, co-condensation approach, post-synthesis grafting, cisplatin

1. Introduction

Since its accidental discovery by Rosenberg *et al.* in 1969, cisplatin (*cis*-diaminedichloroplatinum(II), CDDP) is one of the most widely used and effective cytotoxic agents in the treatment of almost 50 % of cancers[1–3]. It is currently used in combination with other drugs, against cancers of the head and neck, ovaries, esophagus, stomach, colon, testis, cervix and uterus, and as second line chemotherapy against most other advanced cancers, such as pancreas, liver, kidney, prostate, glioblastomas and metastatic melanomas[4]. However, the efficacy and usage of cisplatin are restricted due to the emergence of intrinsic and acquired resistance, and side-effects which include neuro- and nephrotoxicity, which are closely related to its lack of tumor selectivity[5].

In order to provide a higher accumulation of platinum drugs in cancer cells and to minimize the side effects, numerous organic nanometer-sized cisplatin delivery systems have been developed, including polymeric micelles[6], liposomes[7] and cisplatin pro-drug nanoparticles[8]. In addition, different inorganic materials[9] with unique and interesting properties such as gold nanoparticles[10], iron oxide nanomaterials[11] and carbon nanotubes[12] have been explored for delivering platinum-based drugs. Over the last two decades, mesoporous silica nanoparticles (MSNs) have attracted extensive attention to overcome challenges in current cancer treatments due to their unique physico-chemical properties such as biocompatibility, ordered pore network, chemical stability, tunable pore diameters (2 nm to 10 nm), high pore volume (~1 cm^3/g) and high surface area (800 m^2/g)[13,14]. Moreover, these materials can be functionalized either inside or outside the pore channels by using a co-condensation approach or a post-synthesis modification with various organic linkers, including mercapto groups, thereby simplifying the design of controlled-release mechanisms and improving the solubility of poorly water-soluble drugs[15–20].

To increase the biocompatibility and reduce undesired interactions between the biological environment and the nanocarriers, the functionalization of the outer MSNs surface with poly(ethylene glycol) (PEG) has been investigated by covalent grafting[21,22]. This approach

has been highly used to avoid clearance of the nanoparticles by 'first-pass' organs, such as lung and kidney, prolong their blood circulation half-lives and consequently, increase their accumulation in the targeted tissues. PEG modification also increases the dispersion and thus the stability of the nanoparticles under physiological conditions[23]. Dispersion of nanoparticles through electrostatic repulsion can also be achieved by grafting the nanoparticle surface with charged polymers to achieve sufficient electrokinetic potential to obtain repulsion at the desired conditions. Among them, polyethyleneimine (PEI) has been one of the most widely used cationic dispersant and gene transfection agent due to its strong DNA condensation capacity and intrinsic endosomolytic activity[24–28]. Although inefficient for gene delivery but less toxic than high molecular weight PEI, coating of MSNs with low molecular weight PEI polymers has been used to increase delivery of paclitaxel into cancer cells[29]. For CDDP delivery, the introduction of low molecular weight PEI (M_w = 800 g/mol) into CDDP-encapsulated liposomes enhanced cellular uptake and extended cellular retention, thus facilitating DNA exposure to cisplatin[30].

Regarding CDDP delivery using MSNs, Gu *et al.* used the properties of carboxylic groups to coordinate with platinum and form a complex by replacing the chloride ion ligands[31,32]. Later, Lin *et al.* incorporated CDDP-carboxylate complexes with a pH-sensitive hydrazone bond to tether CDDP complexes to the internal surfaces of MSNs, leading to the release of CDDP-carboxylate complexes under endosomal or lysosomal pHs[33]. The effect of amine and carboxyl functionalization of MCM-41 microparticles on the release of cisplatin were also studied by Arean *et al.*[34]. Later, Vivero *et al.* reported the use of folic acid-conjugated MSNs for the delivery of the cisplatin(IV) prodrug[35]. More recently, Huang *et al.* developed MSNs based copolymer composites where cisplatin release was controlled through coordination interaction between carboxyl groups of (poly(MPC-*co*-IA)) and CDDP[36]. Depending on the chemical properties of the materials, CDDP loading generally varied from 0.9 to 26.5 wt%. While dimethylsulfoxide (DMSO) is often used as a solubilizer during the loading process, it has been reported that it inhibited cisplatin cytotoxicity and its ability to initiate cell death[37]. Consequently, the use of DMSO during the loading step must be avoided at all cost. High

adsorption of CDDP has been also observed on mercapto-silylated silica surfaces[38,39]. Although these studies have reported efficient loading and prolonged delivery of cisplatin, the effect of MSNs surface modification using stabilizing or transfection agents, such as PEG or PEI, on the loading and release of CDDP, has not been investigated. Moreover, very limited attention has been directed to the spectroscopic properties and spatial distribution of CDDP once loaded into MSNs.

In the present work, we report the surface functionalization of MSNs with PEG or PEI using a two-step post-synthesis grafting approach (Fig. 1(a-b)). A low molecular weight (1.8 kDa) branched PEI was used because of its low toxicity. Given a strong affinity of sulfur for platinum, thiol-functionalized MSNs were synthetized as a reference using a co-condensation approach (Fig. 1(c)). The nanomaterials were thoroughly characterized by an array of techniques including transmission electron microscopy (TEM), dynamic light scattering (DLS), ^{29}Si magic angle spinning nuclear magnetic resonance (^{29}Si MAS NMR), Raman and Fourier-transform infrared (FTIR) spectroscopies, thermogravimetric analysis (TGA), elemental analysis (EA), X-ray diffraction (XRD) as well as nitrogen sorption measurements. To compare the loading capacity of the functionalized nanomaterials, CDDP was loaded either by adsorption or impregnation of an aqueous solution of CDDP without the use of dimethylsulfoxide (DMSO). CDDP loading was evaluated by scanning electron microscopy (SEM), scanning transmission electron microscopy (STEM) - high-angle annular dark field (HAADF) and Raman spectroscopy measurements. Additionally, preliminary release studies were performed at 37°C in 1 mM NaCl. This study sought to identify an appropriate surface-functionalized MSNs delivery system for further biomedical applications.

2. Materials and Methods

2.1 Materials

Tetraethyl orthosilicate (TEOS, Aldrich), cisplatin (CDDP, Aldrich), *n*-cetyltrimethylammonium bromide (C_{16}TAB, Aldrich), standard solution of sodium hydroxide (2 M NaOH, Aldrich), ammonium nitrate (NH_4NO_3, Fisher Chemicals, ≥ 99.0 %), hydrochloric acid (HCl, Fisher Chemicals, 35-38 %), ethanol (C_2H_5OH, Fisher Chemicals, 95 %), (3-mercaptopropyl)triethoxysilane (MPTES, Fluorochem), (3-triethoxysilyl)propylsuccinic anhydride (TESP, Fluorochem), poly(ethylene glycol) monomethyl ether amine ($mPEG_{10000}$-NH_2, M_W = 11,153 Da, Iris-Biotech), polyethylenimine (PEI_{1800}, MW = 1800 g.mol^{-1}, 50 % (w/w) in water, Aldrich), N-hydroxysuccinimide (NHS, Aldrich, 98 %), (1-ethyl-3-[3-dimethylamnipropyl])carbodiimide hydrochloride (EDC, Aldrich), cisplatin (CDDP, Aldrich, ≥ 99.9 %), orthophenylenediamine (OPDA, Aldrich, ≥ 98.0 %), dimethylformamide (DMF, Aldrich, HPLC grade), dichloromethane (DCM, Aldrich, HPLC grade), diethylic ether (DE, Aldrich, HPLC grade) and RPMI 1640 medium (Biowhittaker) were used without further purification. Chemical modification of MSNs was performed in dry toluene (homemade distillation). Ultrapure water (18 MΩ.cm) was used for all synthesis and purification steps (pure UHQ, Elga, France).

2.2 Synthesis of pure MSNs

Bare mesoporous silica nanoparticles (MSNs) were prepared according to our previous procedure[40,41]. Briefly, 416.6 mg of CTAB (1.14 mmol) were dissolved in 200 mL of water in a 500 mL four-neck round bottom flask. The solution was purged thrice with a N_2 flow (1 L.min^{-1}) and a 2 M NaOH standard solution protected from ambient air (1.45 mL, 2.90 mmol) was added under the same N_2 flow. After stirring for 2 h at 70°C under a N_2 flow of 150 mL.min^{-1}, 2.01 mL of TEOS were added at 1 mL.min^{-1} under a N_2 flow of 1 L.min^{-1}. The molar composition of the solution was 1 TEOS: 0.32 NaOH: 0.127 C_{16}TAB: 1235 H_2O. After 2 h of stirring, the pH of the colloidal suspension was adjusted to 7.5 by adding 1 M HCl solution. The mixture was stirred for another 24 h under static N_2 atmosphere. The sample

was separated by centrifugation (25 000*g*, 20 min, 20°C). The solid cake was redispersed in ultrapure water using an ultrasonic cleaner for 1 min. The centrifugation-redispersion procedure was repeated until the conductivity of the supernatant was lower than 10 µS/cm. Water was then slowly removed by rotary evaporation at 80°C for 1.5 h. The sample was heated at 90°C under vacuum for 1 h to ensure the complete removal of the solvent. The template was extracted by using the chemical route proposed by Lang *et al.* in order to prevent irreversible aggregation of nanoparticles observed with calcination . Typically, 600 mg of MSNs were refluxed in a NH_4NO_3/EtOH (2 g/100 mL) mixture for 1 h. This procedure was repeated four times and centrifugation (12 000*g*, 10 min, 20°C) was used to wash the particles between each step. At the end of this process, MSNs were then extensively rinsed with ethanol. After complete removal of the solvent under vacuum, the powder was stored in a desiccator. In these storage conditions, structural properties of the MSNs are preserved at least 8 months. These mesoporous nanoparticles were referred to as MSNs.

2.3 Grafting of carboxylic groups at the surface of MSNs by silanization (MSNs-COOH)

Mesoporous silica nanoparticles were first synthesized according to the procedure described for pure MSNs until the centrifugation-redispersion step. Then, the nanoparticles were dispersed in ethanol. In order to remove adsorbed surfactants at the surface of the nanoparticles, a Soxhlet extraction has been performed in ethanol for 24 h (Fig. 1(a)). The resulting nanoparticles were then collected by centrifugation (12 000*g*, 10 min, 20°C), washed, redispersed with deionized water and finally freeze-dried. Grafting of carboxylic groups on the surface of MSNs was performed according to a reported procedure published for mesoporous materials[43,44]. Briefly, 150 mg of lyophilized MSNs were degassed under vacuum for 12 h and suspended in 15 mL of dry toluene. Then, 34 µL of TESP (120 µmol) were added dropwise to the mixture. After 24 h of stirring under static N_2 atmosphere, the obtained solid was washed 3 times with a mixture of diethyl ether and dichloromethane (1:1, v/v) and finally dried at 60°C for 12 h in air. The template was then extracted by using the method described for pure MSNs. After complete removal of the solvent under vacuum,

the powder was stored in a desiccator. These nanoparticles were referred to as MSNs-COOH.

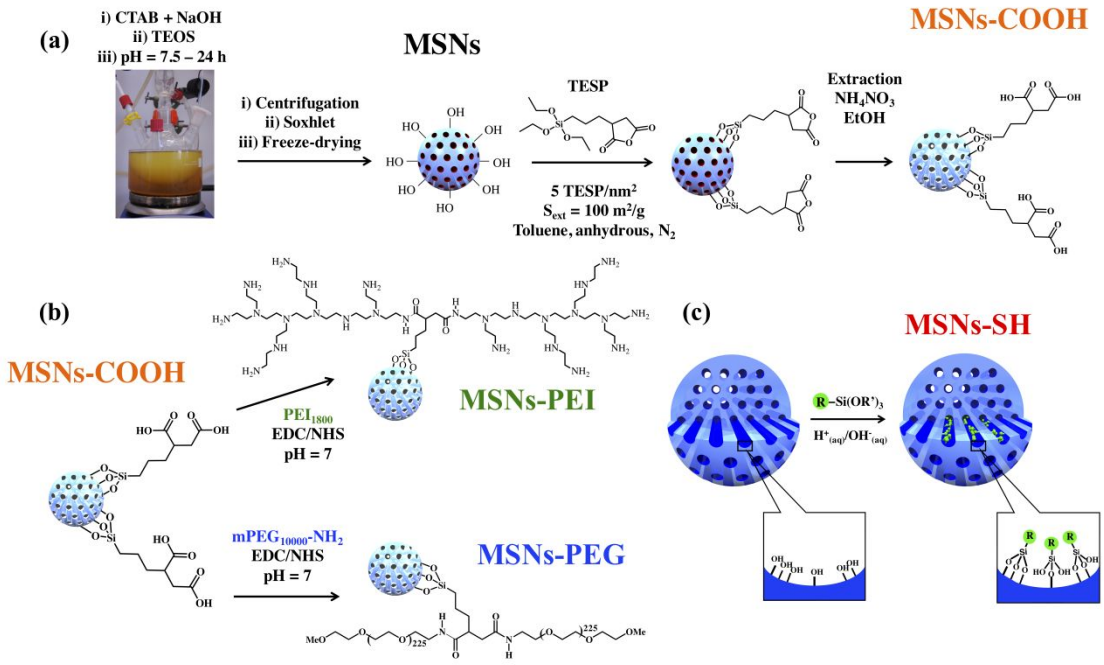

Figure 1: Modification of mesoporous silica nanoparticles by (a) surface grafting of carboxylic groups (MSNs-COOH) by post-synthesis modification with (3-triethoxysilyl)propylsuccinic anhydride (TESP), (b) coating of polyethylene glycol (PEG) and polyethyleneimine (PEI) by amidation (namely MSNs-PEG and MSNs-PEI, respectively) and (c) co-condensation with (3-mercaptopropyl)triethoxysilane (MPTES) leading to MSNs-SH. R = -(C_3H_6)SH and R' = -(OCH_2CH_3)$_3$.

2.4 Coating of polymers by amidation (MSNs-PEI and MSNs-PEG)

PEI_{1800} or $mPEG_{10000}$-NH_2 were grafted to MSNs-COOH in the presence of EDC and NHS (EDC:COOH = NHS:COOH = 2:1) (Fig. 1(b)). The molar composition was 1 COOH: 5 NH_2: 10 EDC: 10 NHS. In a typical procedure, 100 mg of NHS were dissolved in DMSO before adding 5 mL of ultrapure water, EDC (160 mg dissolved in 5 mL of ultrapure water) and 10 mL of MSNs-COOH suspension (150 mg in 10 mL of water, pH = 7). To this, PEI_{1800} (450 mg of a solution at 50 % in weight) or $mPEG_{10000}$-NH_2 (4.8 mg) dissolved in 5 mL of

water were subsequently added to the reaction mixture and let stirred for 24 h at 20°C. The resulting nanoparticles were then intensively washed with ultrapure water. After complete removal of the solvent under vaccum, powders were stored in a dessicator. The nanoparticles were referred to as MSNs-PEI and MSNs-PEG.

2.5 Synthesis of mercapto-functionalized mesoporous silica nanoparticles (MSNs-SH)

The synthesis of MSNs-SH was achieved by a co-condensation procedure using the same protocol as described above for pristine MSNs. The mixture containing the organoalkoxysilane precursor (MPTES) and TEOS was added to the CTAB solution under N_2 flow of 1 L.min^{-1} (Fig. 1(c)). The amount of organoalkoxysilane was 10 mol% of the total amount of silane. The pH aging process, product isolation and surfactant removal were carried out by the method described above except that at the end of the template removal process, a supplementary step was processed by redispersing the pellet in a solution of 10 mL concentrated hydrochloric acid in 100 mL of ethanol. After refluxing for 1 h, the MSNs-SH were separated by centrifugation (12 000*g*, 10 min) and extensively washed with ethanol. After complete removal of the solvent under vaccum, the powder was stored in a desiccator. These nanoparticles were referred to as MSNs-SH.

2.6 Physico-chemical characterizations of the nanomaterials

MSNs samples were characterized by nitrogen physisorption analysis at 77 K using a Micromeritics ASAP 2020 setup. Samples were degassed prior analysis at 363 K. The specific surface area (S_{BET}) of the materials was calculated using BET method in the relative pressure range between 0.06 and 0.25. The pore-size distribution (D_p) and pore volume (V_m) were determined from the desorption branches of the isotherms using the BJH-method at $P/P_0 \leq 0.75$ in order to remove the contribution of interparticle mesoporosity. The structural properties of the samples were characterized by low angle powder X-Ray Diffraction (XRD) using a Bruker D8 Advance diffractometer equipped with Vantec linear PSD, using CuK_α radiation (35 kV, 35 mA). The diffraction patterns were recorded over the range 0.5°-10° (2θ), with a 0.017° step and a step time of 3 s. The hydrodynamic diameter of the particles

was measured by Dynamic Light Scattering (DLS) at 173° angle using a Malvern Nano ZS instrument (Malvern Instruments, UK) equipped with a 4 mW He-Ne laser (λ = 633 nm). The mean particle size, D_H, was obtained from a fit of a single exponential to the correlation function with the corresponding polydispersity index (PDI). Each measurement was carried out in triplicate. The plotted data are mean values of the three independent measurements. Zeta potential measurements were performed on a zeta-Nanosizer (Malvern Instruments, UK) supported by a DTS Nano V6.20 software. The nanomaterials were dispersed in 10^{-2} M NaCl aqueous solutions at around 1 mg/mL. The pH of the solution was adjusted from 3 to 11 by addition of HCl or NaOH solutions. The decomposition of organic species was studied by thermogravimetric analysis (TA instruments, Discovery, USA). The heating rate was 2 °C.min^{-1} from 25°C to 800°C under air flow (25 mL.min^{-1}). Sample weight was around 5-10 mg. Precision of the instrument is 0.1 wt%. The elemental analysis of the materials was obtained from a Thermo Scientific Flash EA 1112 HT. The morphology and the mesostructure of the prepared materials were characterized using a Transmission Electron Microscope (TEM, JEM2100 LaB_6 cathode, JEOL, Japan) operating at 200 kV and fitted with a high tilt pole piece achieving a point-to-point resolution of 0.25 nm. A drop of the diluted suspension was placed on a 300-mesh carbon film coated copper grid. After solvent evaporation (ethanol), the size of 100 particles was measured to determine the intensity-weighed mean diameter of the particles, d_{TEM}. FTIR characterizations of dried powders were performed at room temperature using a Bruker Equinox 55. Dried powders were disposed between 2 pellets of KBr. Solid-state nuclear magnetic resonance (NMR) experiments were performed on an ASX 400 spectrometer (Bruker) operating at a Larmor frequency of 79.49 MHz. The samples were placed in a 7.5-mm MAS probe and spun at 10 kHz. To obtain quantitative spectra for all samples, single-pulse excitation with continuous decoupling was used for ^{29}Si MAS NMR, with a 5 µs $\pi/6$ pulse duration and a recycle delay of 60 s. ^{29}Si CP MAS NMR spectra were used to fix chemical shifts and were acquired with a 5 s recycle delay, 2 µs $\pi/6$ (^{1}H) pulse duration and 3 ms contact time. It was checked that no relaxation

effect could affect relative line intensities in ^{29}Si experiments; a recycle delay of 240 s did not lead to any change in the relative ratio of the individual components as obtained from spectral decomposition. Solid-state NMR spectra were reconstructed using Dmfit software[45]. The Raman spectra of MSNs-SH were recorded using a Renishaw InVia setup with a 532-nm incident laser wavelength. Conversely, loaded-MSNs were characterized as follows. STEM-HAADF micrographs were taken on a JEOL JEM 2100F instrument equipped with a FEG type cathode operating at 200 kV. Scanning electron microscopy (SEM) was performed using a JEOL JSM 7600F instrument. Samples for SEM were prepared by dispersing the powders on the conductive carbon tape. For Raman spectroscopy of the loaded samples, a 785-nm incident laser wavelength was used instead to avoid photoluminescence.

2.7 Loading of cisplatin by adsorption or impregnation

To study the adsorption capacity of the nanomaterials, CDPP (20 mg) was completely dissolved in 20 mL of water (1 mg/mL) and aged for 6 h in order to get its first hydrolysis product $[Pt(NH_3)_2Cl(OH_2)]^{+}$[46]. Then, the prepared MSNs-SH, MSNs-PEI, MSNs-PEG and pure MSNs (100 mg) were added to the CDDP solution (100 mg of MSNs/20 mg CDDP) and sonicated. After stirring for 18 h in the dark at 20°C, the resulting suspensions were centrifuged (25 000*g*, 15 min, 20°C). Supernatants were then collected and the CDDP content was determined by derivatization with *o*-phenylenediamine (OPDA) as previously described with slight modifications[47]. In a typical procedure, 100 µL of a CDDP solution (standards or supernatants) were mixed with 30 µL NaCl solution (5 M in water) and 870 µL ultrapure water. The solution was kept in the dark for 5 days at 20°C. Then, 1 mL of OPDA solution (2.15 mg/mL in DMF) was added and the mixture was heated for 30 min at 90°C, allowed to cool down, and then the volume was completed to 10 mL with a mixture of DMF and water (7:3, v/v). The maximum absorbance of the product was then recorded at 705 nm (UV-2550, Shimadzu, Japan). For loading cisplatin by impregnation, the same protocol used to load CDDP by adsorption was applied, except that the resulting suspensions were dried in the dark at 40°C for 24 h after the adsorption step. Then, the resulting powders were collected and dispersed in ethanol. After 15 min of settling, the supernatants were collected

and centrifuged (25 000*g*, 15 min, 20°C). Finally, the loaded nanomaterials were dried under vacuum and the CDDP content was measured by inductively coupled plasma atomic emission spectroscopy (ICP-AES) performed on an Analytik Jena AG contra 700 instrument.

3. Results and discussion

3.1 Overall description of the functionalization methods

Non-functionalized pure-silica MCM-like materials (pristine MSNs) were synthesized according to our previous procedure leading to stable colloidal suspensions of nanoparticles with a diameter of 160 nm and with a high structural stability[40,41]. As described in Fig. 1(a), Pristine MSNs were then coated by the reaction between MSNs free hydroxyl groups and (3-triethoxysilyl)propylsuccinic anhydride, to afford carboxyl-functionalized MSNs (MSNs-COOH). This step was performed in dry toluene after eliminating the template at the surface of the nanoparticles using a Soxhlet extraction. After freeze-drying the nanoparticles without altering the structure, the nanohybrids (MSNs-COOH) were coupled with amino-terminated-PEG chains (PEG-NH_2) or low molecular weight branched PEI by EDC coupling, to afford MSNs-PEG or MSNs-PEI[48,49] (Fig. (1(b)). A co-condensation approach was also employed to introduce mercaptopropylsilane into the silica networks[50,51] (Fig. 1(c)).

3.2 Physico-chemical properties of PEG or PEI-functionalized mesoporous nanomaterials

TEM analysis showed that the surface-functionalized nanoparticles were flattened spheres, a morphology similar to that of pristine MCM-41 nanoparticles, proving that the surface modification did not affect the morphology (Fig. 2(a-d and Fig. S1(a-d)). TEM images also did not reveal the presence of bonds between particles (Fig. 2(a-d)) and DLS showed narrow particle size distributions (Fig. 2(e)). The size of functionalized MSNs was very similar to that of pristine MSNs (d_{TEM} ~ 150 nm and D_H ~ 200 nm), indicating that no aggregates were formed during the modification procedures (Table 1). The nanoparticles were rather monodispersed in size as demonstrated by PDI and c_v lower than 0.23 and 0.20, respectively (Table 1). In addition, MSNs-PEI and MSNs-PEG were colloidally stable for several days in an aqueous solution containing 1 mM NaCl, pH = 7 (Fig. S2).

X-Ray diffraction (XRD) patterns further confirmed the typical structure of MCM-41 materials (Fig. S3). Well-defined (100) peaks, along with the (110) and (200) peaks, characteristic of the 2D hexagonal mesoporous structure were observed, indicating that the surface modification procedure, including the Soxhlet and freeze-drying steps, did not alter either the MCM-41-like structure or the lattice parameter a_0 (Table 1). The honeycomb-like mesoporous structure was also confirmed by TEM (Fig. 2).

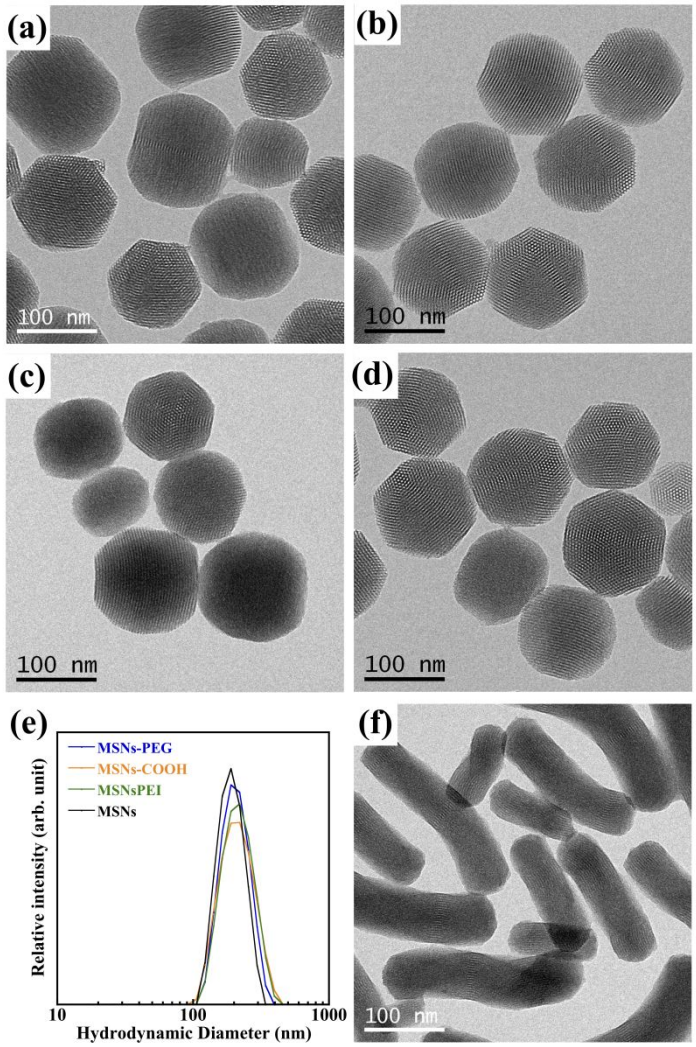

Figure 2: TEM images of (a) pure MSNs (MSNs), (b) MSNs-COOH, (c) MSNs-PEI, (d) MSNs-PEG, (e) the corresponding size distributions obtained by DLS and (f) TEM image of MSNs-SH.

Table 1: Properties of the functionalized mesoporous silica nanoparticles.

Sample	***D_H[a] (nm) (PDI[b])***	***d_{TEM}[c] (nm) (c_v[d])***	***a_0[e] (nm)***	***S_{BET}[f] (m^2/g)***	***V_m[g] (cm^3/g)***	***D_p[h] (nm)***	***τ_{TGA}[i] (molec/nm^2) (mmol/g)***	***τ_{EA}[j] (molec/nm^2) (mmol/g)***
MSNs	221 (0.23)	130 (0.20)	4.85	1062	0.96	2.8	-	-
MSNs-COOH	203 (0.10)	142 (0.14)	4.70	904	0.75	2.6	1.21COOH 0.56	1.48COOH 0.69
MSNs-PEG	197 (0.05)	139 (0.15)	4.74	455	0.31	2.2	0.10PEG 0.02	0.09PEG 0.02
MSNs-PEI	224 (0.22)	144 (0.17)	4.68	580	0.39	2.1	0.50PEI 0.08	0.74PEI 0.12
MSNs-SH	-	70(L)/327(l) (0.21(L)/0.36(l))	4.17	1225	0.75	2.3	0.67SH 1.36	0.61SH 1.20

[a] D_H: mean size of the extracted nanoparticles. [NaCl] = 10^{-3}M. Data are means of three independent measurements.

[b] PDI: polydispersity index (width of the distribution) from the Cumulants analysis.

[c] d_{TEM}: mean TEM diameter calculated by measuring 100 particles ($\Sigma d_i^6/\Sigma d_i^5$). (L) and (l) represent the width and the length of the particles, respectively.

[d] c_v: relative standard deviation, $c_v = \sigma/d_{TEM}$ where σ is the standard deviation of the distribution.

[e] a_0: lattice parameter ($a_0 = 2d_{100}/\sqrt{3}$) where d_{100} represents the spacing of (100) for the extracted samples.

[f] S_{BET}: BET specific surface area calculated in the relative pressure range between 0.06 and 0.25.

[g] V_m: pore volume calculated at $P/P_0 \leq 0.75$ in order to remove the contribution interparticle mesoporosity.

[h] D_p: BJH pore diameter calculated from desorption branch.

[i] τ_{TGA}: Determined by TGA by subtracting the weight loss determined for pristine MSNs (for MSNs-SH and MSNs-COOH) or MSNs-COOH (for MSNs-PEG and MSNs-PEI).

[j] τ_{EA}: Determined by EA. Relative elemental contents of carbon, sulfur and nitrogen were used respectively for MSNs-PEG/MSNs-COOH, MSN-SH and MSNs-PEI. Specific surface area of 560 m^2/g and 100 m^2/g were considered for MSNs-COOH and MSNs-PEG/PEI, respectively. Subtraction of carbon contents with the corresponding materials were used to determine the grafting densities of MSNs-COOH, MSNs-PEG and MSNs-PEI.

The textural properties of pristine and functionalized-MSNs were evaluated by nitrogen adsorption-desorption technique. BET (Brunauer-Emmet-Teller) and BJH (Barrett-Joyner-Halenda) methods were used to calculate the surface area (Table 1) and plot the pore size distribution (Fig. S3). Type IV isotherms were observed for all samples with a sharp capillary condensation step between 0.2 – 0.4 p/p_0 (Fig. S3). A hysteresis loop at high relative pressure (~0.9) was observed and attributed to inter-particle porosity. After addition of carboxylic silane, the sorption properties of the nanomaterials did not change significantly since the specific surface area (S_{BET}) slightly decreased from 1062 m^2/g to 904 m^2/g, the pore volume (V_m) from 0.96 to 0.75 cm^3/g and the pore diameter (D_p) from 2.8 to 2.6 nm (Table 1). However, after polymer grafting, N_2 adsorption isotherms showed a significant decrease of the capillary condensation step at 0.2 – 0.4 p/p_0 which also shifted to lower pressure. Consistently, S_{BET}, V_m and D_p drastically decreased (Table 1). It shows that part of the pores is not accessible anymore or some pores have been partially obstructed, suggesting that the grafting has occurred both at the external surface of the MSNs and slightly inside the pores. Sorption studies performed on pristine MSNs after Soxhlet extraction corroborate this latest point. Indeed, the high specific surface area after Soxhlet extraction (S_{BET} = 560 m^2/g) indicates that the condensation of the carboxylic silane was partly possible at the entrance of the pores, allowing subsequently the grafting of the polymer inside the channels of MSNs.

ζ-Potential measurements indicated an Isoelectric point (IEP) at 3.8 for pure-MSNs, which is in good agreement with previous reports[52,53] (Fig. 3(a)). ζ-potential of MSNs measured at pH7 shifted from positive (+30 mV) to negative (-30 mV) after the Soxhlet extraction (not shown), thus proving the surface of the MSNs was free of surfactants. ζ-potential of MSNs-COOH was negative along the range of pH, confirming the presence of acid groups onto the surface of MSNs. For MSNs-PEI, the IEP shifted at pH 9.6 reflecting the presence of basic groups onto the surface of MSNs. This value is in good agreement with the literature[24,54].

Neutral polymer like PEG was grafted at the surface of the MSNs as potentials were very close to 0 mV along the range of pH (Fig. 3(a)).

Grafting densities were determined using TGA and EA. Thermogravimetric analyses of the materials are presented in Fig. 3(b) (started at 130°C to compensate for different water losses) and Fig. S4 (full analyses with derivatives). As described for pristine MSNs (Fig. S4), the weight losses between 25-150°C and 150-400°C were respectively attributed to physisorbed and chemisorbed water (8 and 4.2 %, respectively) and corresponds to 3.7

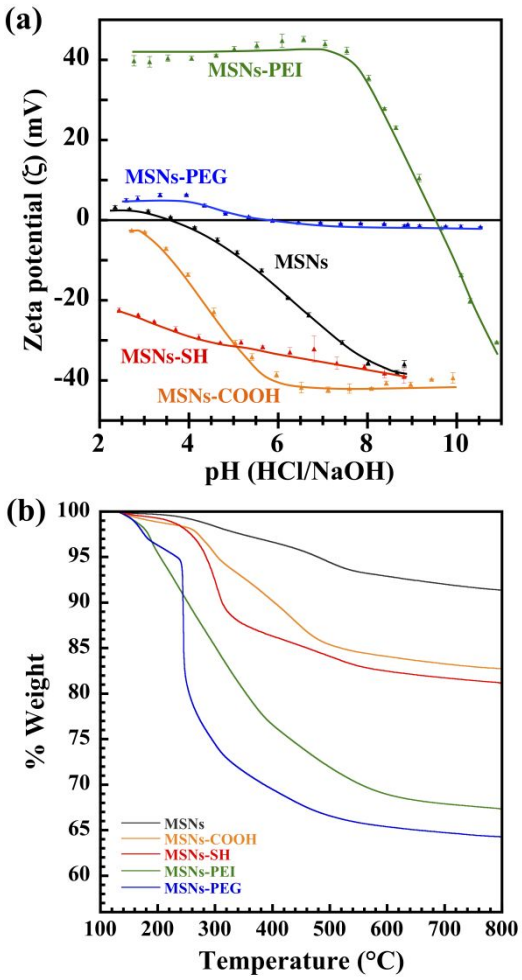

Figure 3: Properties of the functionalized mesoporous nanoparticles obtained by (a) zeta potential measurements and (b) thermogravimetric analysis (starting at 130°C to compensate for different water losses). [NaCl] = 10^{-2} mol.L^{-1} for zeta potential measurements.

molecules of H_2O per nm^2, in good agreement with the literature[55]. The weight loss after 400°C was attributed to the condensation of silanol groups which can occur until 1100°C[56]. For functionalized-MSNs, the weight losses between 25-150°C due to physisorbed water were lower than that of pristine MSNs. The weight losses due to the presence of the functional groups generally occurred between 200°C and 600°C (Fig. S4). For MSNs-COOH, the weight loss observed before 200°C was attributed to the formation of the succinic anhydride[57]. For MSNs-COOH, the grafting density was calculated by subtracting the weight loss determined for pristine MSNs at 200°C. For MSNs-PEG and MSNs-PEI, such subtraction was performed using MSNs-COOH at 70°C. Grafting densities obtained by TGA and EA were in very good agreement and varied from 0.02 to 0.69 mmol/g or from 0.09 to 1.48 molec/nm^2 depending on the functional group (Table 1). Compared with the number of PEI/nm^2, the number of PEG/nm^2 was very low (only 6 % of carboxylic groups were used) and is attributed to the greater steric hindrance and coiling and consequently less effective surface binding of the PEG-NH_2 to the carboxylic surface[35]. FTIR spectroscopy was used to confirm the presence of the functional groups as well as the amide formation (Fig. 4(a)). For all samples, FTIR showed typical bands of the silica framework[58] between 1300 cm^{-1} and 500 cm^{-1} (Fig. 4(a)): ν_{as}(O-Si-O) at 1078 cm^{-1}, ν_s(O-Si-O) at 807 cm^{-1}, ν_{as}(Si-O-Si) at 1221 cm^{-1} and ν(Si-OH) at 970 cm^{-1}. PEI vibrations observed at 2938 cm^{-1} (C-H asymmetric stretching) and 2846 cm^{-1} (C-H symmetric stretching) were identified on both PEI and MSNs-PEI spectra while missing for pure MSNs spectrum (Fig. 4(a)), highlighted by double stars)[59]. Similarly, PEG vibrations were identified on PEG and MSNs-PEG spectra while missing from pure MSNs spectrum: C-H stretching modes of the methyl and methylene groups of the polymer chain between 2980-2880 cm^{-1} (three stars), CH_2 wagging at 1340 cm^{-1} (four stars) and CH_2 scissoring at 1465 cm^{-1} (five stars)[23]. For all spectra, the bending mode vibration of water[60] is observed at 1628 cm^{-1}. In addition, C=O stretching vibration at 1719 cm^{-1} (single star) was only observed for MSNs-COOH and MSNs-PEG and confirmed our TGA/EA results showing that a low number of carboxylic groups was used for the conjugation with

PEG. Disappearance of this vibration band for MSNs-PEI highlighted that more carboxylic groups was used for the conjugation with PEI. For both MSNs-PEG and MSNs-PEI, the band observed at 1700 cm^{-1} could be characteristic of the free remaining carboxylic groups. Finally, vibrations around 1550 cm^{-1} (1558 and 1569 cm^{-1} for MSNs-PEI and MSNs-PEG, respectively), assigned as Amide II (N-H bending and C-N stretching), were observed for MSNs-PEG and MSNs-PEI, thus proving successful amide bond formation[61,62]. Solid state ^{29}Si MAS NMR provided information about the silicon environment and the degree of functionalization. Cross-polarized ^{29}Si MAS NMR (qualitative) was first used to settle chemical shifts (Fig. 4(b)), allowing to determine peak areas obtained using a single pulse

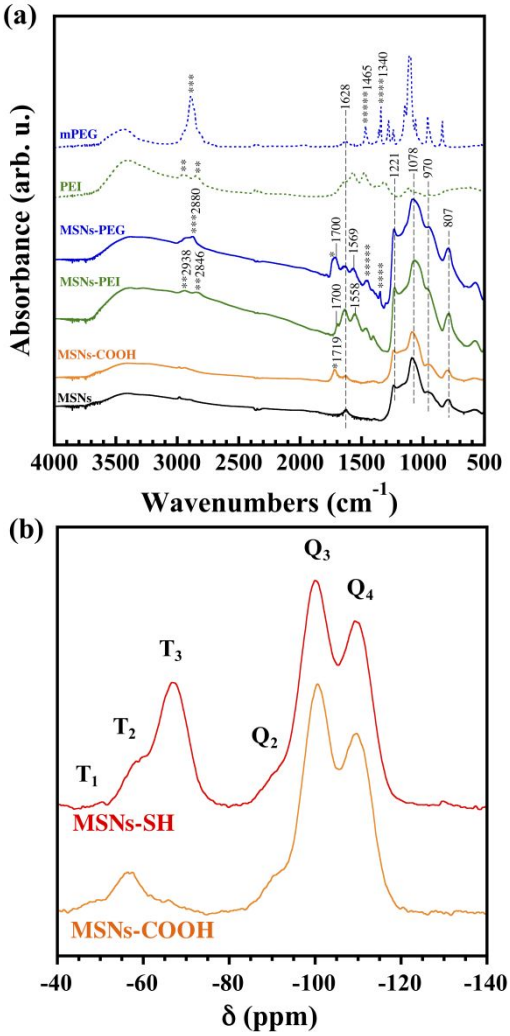

Figure 4: Spectroscopic characterizations of the mesoporous silica nanoparticles by (a) FT-IR performed under air and (b) Cross-polarized ^{29}Si MAS NMR.

experiment (Fig. S5). For MSNs-COOH, typical resonances of Q^{2-4} ($Q^n = (SiO)_n(OH)_{4-n}$) for the siloxane moieties were observed at -91 (Q^2), -100 (Q^3) and -110 (Q^4) ppm. As expected, the grafting process resulted in a decrease in the intensity of the Q^3 resonance and a concomitant increase in the intensity of the Q^4 resonance (Fig. S5). Consequently, the ratio of the relative peak areas of the deconvoluted peaks, Q^4/Q^3, increased from 1.6 to 1.9 with the functionalization. Upon grafting the surface with carboxylic groups, the ^{29}Si MAS NMR spectrum showed three additional resonances corresponding to the incorporated organosilanes ($T^m = RSi(OSi)_m(OH)_{3-m}$, m=1-3) observed at -48 (T^1), -58 (T^2) and -67 (T^3) ppm.

3.3 Physico-chemical properties of the thiol-functionalized MSNs

By introduction of thiol groups in mesoporous silica using a co-condensation approach, anisotropic nanoparticles were formed, as observed by TEM (Fig. 2(f) and Fig. S1(f)). The diameter of the rods was highly uniform with a size of 70 nm (c_v = 0.21) while the length was 327 nm (c_v = 0.36) (Table 1). Due to the anisotropic shape of the nanoparticles, DLS was inappropriate. The pore system appeared to be well-ordered at a local scale with parallel pores aligned to the long axis of the rods (Fig. 2(f)). Such morphology has been already observed by several authors[50,63,64]. Sadasivan *et al.* proposed that repulsive interactions between the negatively charged cylinder walls and soluble deprotonated thiol-containing silica surfactant micelles, along with steric hindrance due to disulfide linkages would favor the particle growth along the channel direction to produce nanofibers with a hexagonal cross-section[63]. The diffraction pattern and sorption isotherm were also typical of ordered MCM-41 type materials (Fig. S3). Compared to pristine MSNs, a reduction in the pore diameter D_p and lattice parameter a_0 was observed (Table 1), while the specific surface area was higher (1225 m^2/g). As previously observed in the literature[65,66], ζ-potential measurements exhibited negative potentials for MSNs-SH over the range of pH (Fig. 3). Grafting densities determined by TGA and EA were in very good agreement and showed that the nanoparticles contained 1.2 mmol/g or 0.6 SH/nm^2 (Table 1).

Raman spectroscopy is much more sensitive to thiols groups than FTIR spectroscopy due to the small dipolar moment[67]. For this reason, the spectroscopic properties of MSNs-SH were determined by Raman instead of FTIR spectroscopy (Fig. S6). First of all, Raman bands of silica were observed for both MSNs-SH and MSNs : 486 cm^{-1} (vibration of tetra cyclosiloxane rings), 800 cm^{-1} (symmetric stretching modes of SiO_4 units (Si-O-Si)) and 978 cm^{-1} (vibration associated with the Si-OH stretching mode of the surface hydroxyls)[50]. In addition, as described in Fig. S6(a), the main peaks of the MPTES precursor were identified within the MSNs-SH spectrum : 651 cm^{-1} (Si-C stretching), 1304 cm^{-1} (out of plane CH_2 bending) and 1452 cm^{-1} (CH_2 and CH_3 in plane bending). The Raman band at 509 cm^{-1} assigned to the stretching of the di-sulfur bond demonstrated the dimerization of some thiol groups. This band was also observed in the precursor but with a smaller intensity. The peak at 2581 cm^{-1} assigned to the stretching of the S-H bond were identified in the spectrum of MSNs-SH (Fig. S6(b)). Compared to pristine MSNs, the increase of the peaks between 2800 and 3000 cm^{-1} (CH stretching region) observed for the MSNs-SH spectrum was obvious and demonstrated that thiol groups were potentially grafted to the silica (Fig. S6(b)).

Additional spectroscopic evidence for the anchoring of the thiol groups was obtained from ^{29}Si CP MAS NMR (Fig. 4(b) and Fig. S5). Resonances of Q^{2-4} were observed at -91 (Q^2), -100 (Q^3) and -110 (Q^4) ppm. The ratio of the relative peak areas of the deconvoluted peaks, Q^4/Q^3, was lower than that of pristine MSNs and was 1.4, which suggests a lower polycondensation degree of the silica network. Unlike MSNs-COOH, MSNs-SH showed only T^2 (-58 ppm) and T^3 (-67 ppm) resonances with relative peak areas of 3 and 12 %, respectively. For MSNs-COOH, the relative peak areas for T^1, T^2 and T^3 were 0.4, 2.8 and 0.2 %, respectively, which suggests that mercaptosiloxane moieties were more tightly incorporated to the silica surface compared to carboxysilane moieties.

3.4 Quantification of cisplatin using OPDA derivatization

The relative adsorption capacity of cisplatin in pristine or functionalized MSNs was studied, using a sensitive and simple method allowing the quantification of cisplatin within supernatants. As cisplatin has a low absorbance in the UV region, no fluorochrome and over

time its UV profile drifts due to hydrolysis[46], quantification methods involving derivatization were developed[68]. For instance, Golla *et al*. were first to develop a method based on the derivatization of CDDP using *o*-phenylenediamine (OPDA)[69], giving rise after only 30 min at 90°C to a complex that strongly absorbs at 705 nm. With slight modifications, this method was used. First, its specificity was evaluated by comparing UV spectra of OPDA, MSNs and cisplatin-OPDA (Fig. 5). UV spectrum of the complex showed a strong absorbance peak at 705 nm with no interference. Linearity was studied in the concentration range of 0.55 µM to 27.67 µM by visual inspection of a calibration curve (inset of Fig. 5) and by calculating the regression equation and the correlation coefficient (R^2) using the method of least squares. The correlation coefficient was 0.999, which indicates a good linearity since a regression coefficient $R^2 > 0.998$ is generally considered as evidence of acceptable fit of the data to the regression line[70].

3.5 Loading of cisplatin by adsorption or impregnation

Although CDDP is soluble in DMF (20 mg/mL) or DMAC (18 mg/mL), the use of such solvents during the loading step is to be avoided due to their high toxicity. CDDP is highly soluble in DMSO (350 mg/mL), which is usually well tolerated with no observable toxic

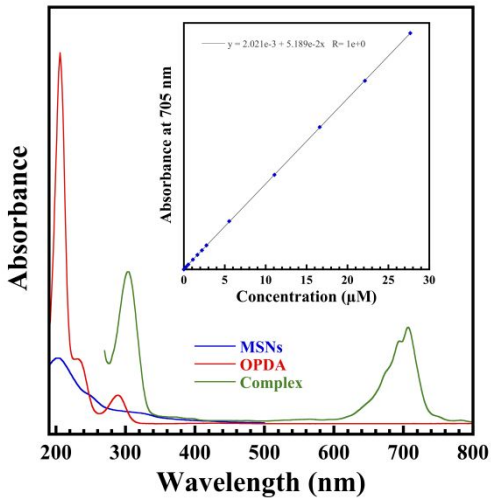

Figure 5: UV-Visible spectra of MSNs, o-phenylenediamine (OPDA) and complex formed by reacting cisplatin with OPDA at 90°C for 30 min in a mixture of DMF:water (1:1, v/v).

effects to cells up to 1 % (v/v). However, the use of DMSO to dissolve CDDP must be prohibited as it has been reported to inhibit its cytotoxicity and its ability to initiate cell death[37]. In the literature, cisplatin loading is generally performed by stirring the nanomaterials at 37°C in an aqueous solution (PBS or water) of CDDP up to 48 h (adsorption). Herein, our nanomaterials were loaded either by adsorption or impregnation. The adsorption study was performed by stirring the nanomaterials at 20°C for 18 h in a 6 h aged solution of CDDP prepared in water at 1 mg/mL. Under these conditions, the most abundant species was its first hydrolysis product $[Pt(NH_3)_2Cl(H_2O)]^+$ according to cisplatin hydrolysis reactions[71]. Results were expressed as the mass percentage of CDDP compared to the total mass of sample (Table 2). The final results for the adsorbed CDDP determined by UV-Vis spectroscopy showed the strongest affinity within the following sequence MSNs-SH (16.09 wt%) > MSNs-PEG (3.32 wt%) > MSNs-PEI (0.99 wt%) > MSNs (0.36 wt%). Compared to the other nanoparticles, MSNs-SH showed the highest amount of adsorbed cisplatin, close to the maximal adsorption value of 16.67 wt%. This result is consistent with the literature showing that the formation of complexes with Pt ions and biological thiols such as GSH, metallothionine and other protein thiols defend the cell against CDDP by limiting the amount of drug available for binding to DNA[72]. Several authors also demonstrated the formation of a strong covalent Pt – S bond after adsorption of CDDP onto mercapto-silylated silica surfaces[38,39]. Compared to pristine MSNs, MSNs-PEG showed greater adsorption capacity, probably reflecting the high electronegativity of the oxygen atoms in the PEG chains. Contrastingly, no significant difference was also observed between pristine MSNs and MSNs-PEI even if the first hydrolysis product of CDPP ($[Pt(NH_3)_2Cl(H_2O)]^+$) is highly reactive to nucleophiles such as amines[73]. This was confirmed by using ICP-AES as a good correlation was observed with the adsorption results determined by UV-Vis spectroscopy (Table 2). At the loading pH, the fact that the amino groups are protonated could limited the amount of adsorbed CDDP. Compared to the literature, our CDDP loadings obtained by adsorption are lower. For instance, under the same loading conditions, Arean *et al.* reported a higher CDDP loading with amino-functionalized MCM-41 (6.1 wt%) materials, despite a

low CDDP loading was obtained with carboxy-functionalized MCM-41 (1.5 wt%)[34]. In their study, the number of complexing sites, which is linked to the number of amino groups introduced in the materials, was considerably higher than that of MSNs-PEI and could explain why the drug loading was higher. While using DMSO during the loading step, different authors also reported high CDDP loading up to 20 wt% using carboxylic groups to coordinate with platinum groups[31,32]. Vivero *et al.* also reported a CDDP loading of 12.5 wt% with pristine MSNs, but still, DMSO was used to load CDDP[74]. Lately, Sun *et al.* described a drug loading capacity of 10.1 wt% by using a nanosized porous/hollow PEI functionalized Gd_2O_3/Fe_3O_4 composite. More recently, Huang *et al.* developed MSNs based copolymer composites and reported an incredibly high drug loading of 26.5 wt% through the use of coordination between carboxyl groups of (poly(MPC-*co*-IA)) and CDDP[36]. In order to increase the drug loading capacity of our nanocarriers, CDDP was loaded by impregnation. The nanomaterials were stirred at 20°C in an aqueous solution of CDDP for 18 h. Then, the suspensions were dried at 40°C for 24 h. The aim was to promote preferential attachment of CDDP within the pores of the MSNs by slowly evaporating the solvent. After washing the nanomaterials, high CDDP loadings were obtained within the following sequence: MSNs-SH (16.07 wt%) > MSNs-PEI (11.30 wt%) > MSNs-PEG (10.07 wt%) > MSNs (3.91 wt%)

Table 2: Amount of adsorbed and impregnated CDDP determined for pristine and functionalized-MSNs. (Pt/Si) distributions were determined by SEM using EDS.

Sample	Adsorbed CDDP[a] (%)	Adsorbed CDDP[b] (%)	Impregnated CDDP[b] (%)	% $(Pt/Si)_{local}$	% $(Pt/Si)_{global}$	Ratio (local/global)
CDDP@MSNs	0.36 ± 0.89	0.82 ± 0.04	3.91 ± 0.20	2.32	7.15	0.32
CDDP@MSNs-PEG	3.32 ± 0.57	2.90 ± 0.15	10.07 ± 0.50	2.83	4.80	0.59
CDDP@MSNs-PEI	0.99 ± 0.38	0.88 ± 0.04	11.30 ± 0.57	6.48	8.01	0.81
CDDP@MSNs-SH	16.09 ± 0.29	16.09 ± 0.80	16.07 ± 0.80	16.57	16.95	0.98

[a]Determined by UV-Vis spectroscopy.

[b]Determined by ICP-AES.

(Table 2). However, due to the loading process employed, some CDDP crystals were expected to be observed outside the pores. Thus, CDDP distribution within the loaded nanomaterials was investigated.

3.6 Cisplatin distribution by SEM, TEM and STEM-HAADF

In the literature, very few studies paid attention to the spatial distribution of CDDP once loaded into MSNs. Herein, CDDP loaded MSNs were characterized by SEM using Backscattered-Electron (BSE) mode (Fig. 6). CDDP crystals (brighter area) with size ranging from few micrometers to 30 µm were observed for all samples, except for CDDP@MSNs-SH. EDS analysis (Fig. 6: arrow number 1) showed that it corresponded to partially hydrolyzed cisplatin as the Pt/Cl atomic ratio was found equal to 0.45 (Pt/Cl = 0.5 without hydrolysis). To estimate the proportion of CDDP remaining outside the nanomaterials, two

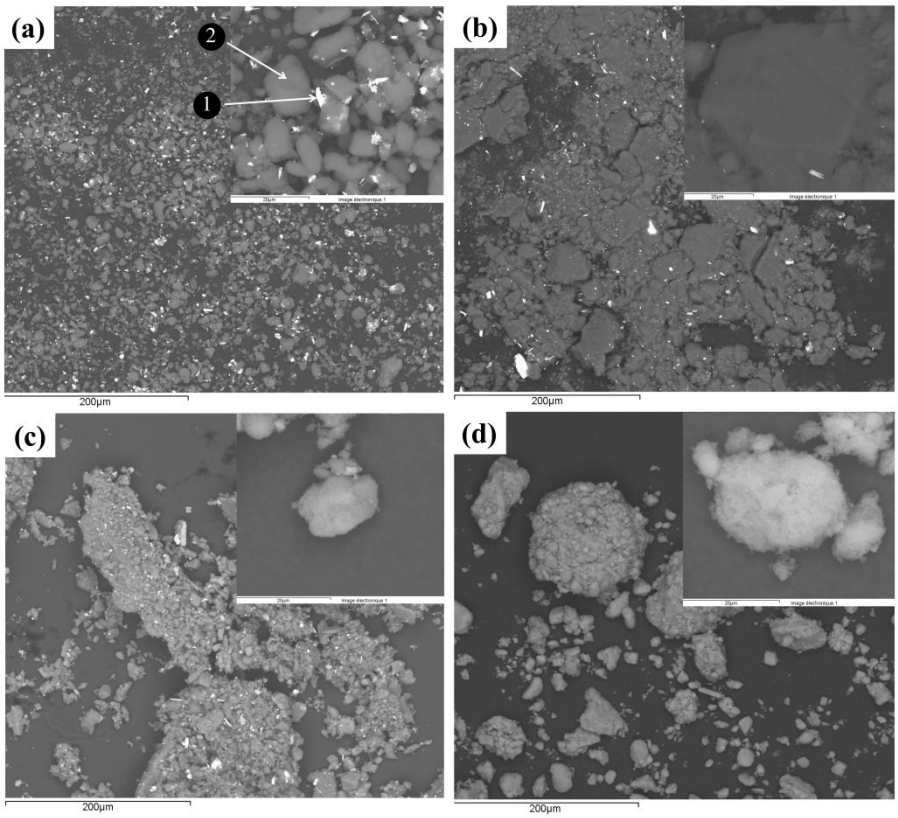

Figure 6: SEM images of (a) CDDP@MSNs, (b) CDDP@MSNs-PEG, (c) CDDP@MSNs-PEI and (d) CDDP@MSNs-SH.

different Pt/Si atomic ratios were determined: $(Pt/Si)_{local}$ and $(Pt/Si)_{global}$. On the one hand, $(Pt/Si)_{local}$ was directly determined on a cluster of loaded-materials nanoparticles taking care to avoid CDDP crystals, as depicted by the arrow number 2 (Fig. 6). On the other hand, $(Pt/Si)_{global}$ was determined on a large zone (around 0.25 mm^2) covering both loaded-materials and CDDP crystals. Then, the homogeneity of cisplatin distribution was evaluated by calculating the following ratio: $(Pt/Si)_{local}/(Pt/Si)_{global}$ (Table 2). The ratio (local/global) showed that the homogeneity decreases within the following sequence MSNs-SH (0.98) > MSNs-PEI (0.81) > MSNs-PEG (0.59) > MSNs (0.32). This trend demonstrated that more CDDP was loaded within the pores of the MSNs-SH, contrary to pristine MSNs. Cisplatin distribution was also characterized at the nanometer scale. For CDDP@MSNs, STEM-HAADF images showed nanocrystals of CDDP (Fig. 7). For the other samples, CDDP was homogeneously distributed (Fig. 7). For CDDP@MSNs, TEM and STEM-HAADF images obtained by tilting the sample along y-axis (0°, +20°, +40°), showed that the nanocrystals of CDDP were aligned with the pores and evidenced that CDDP was encapsulated into the pores (Fig. 8).

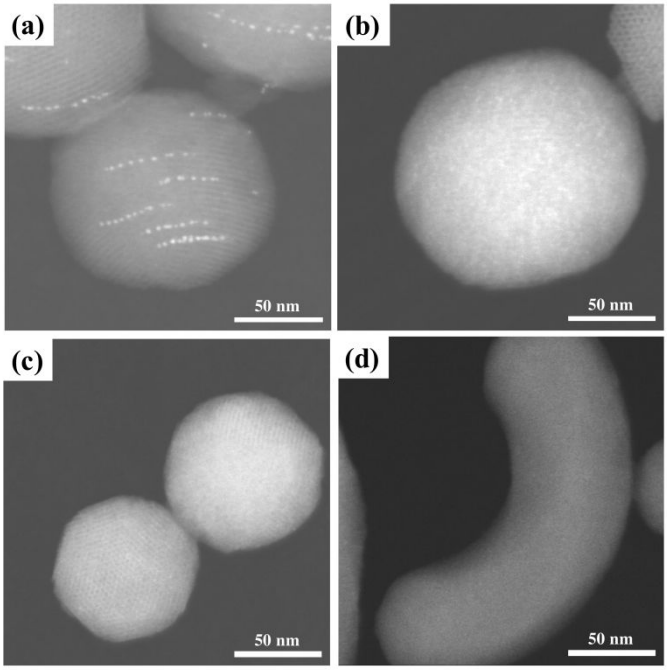

Figure 7: STEM-HAADF images of (a) CDDP@MSNs, (b) CDDP@MSNs-PEG, (c) CDDP@MSNs-PEI and (d) CDDP@MSNs-SH.

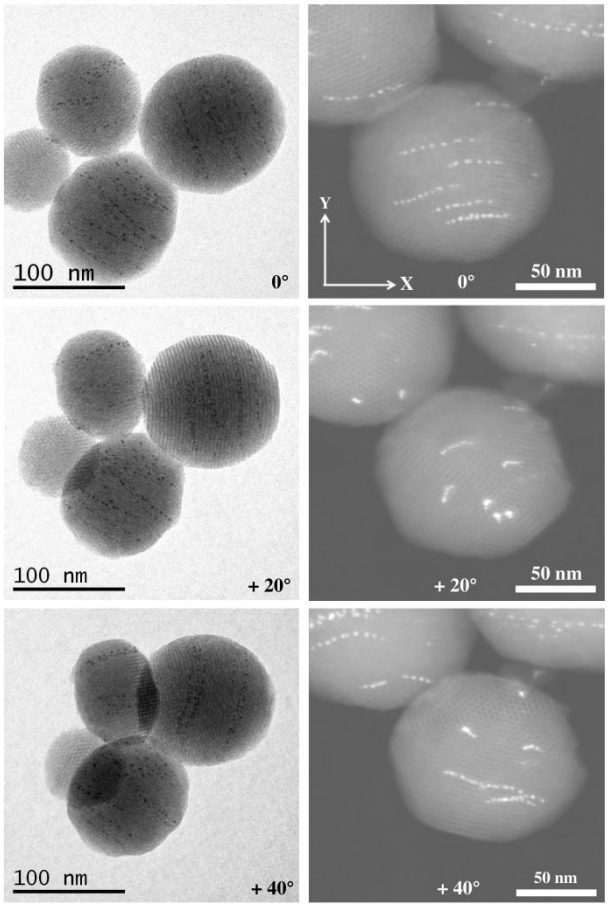

Figure 8. TEM (left) and STEM-HAADF (right) images of CDDP@MSNs after tilting the sample along y-axis.

3.7 Spectroscopic properties of cisplatin-loaded nanomaterials

The Raman spectrum of cisplatin (Fig. 9(a)) showed 4 vibration bands at 162, 255, 322 and 524 cm^{-1} that were respectively attributed to the skeletal in-plane deformation modes $\delta_{Cl\text{-}Pt\text{-}Cl}$, $\delta_{N\text{-}Pt\text{-}N}$ and the Pt-Cl ($\nu_{Pt\text{-}Cl}$) and Pt-N ($\nu_{Pt\text{-}N}$) stretching modes[75,76]. The Raman bands of CDDP were observed for all spectra, except for CDDP@MSNs-SH (Fig. 9(d)) and CDDP@MSNs-PEI (Fig. 9(e)). This confirmed the presence of CDDP either in the pores or outside the particles. For CDDP@MSNs-SH, two broad vibration bands were observed at 310 and 486 cm^{-1}. The vibration band at 310 cm^{-1} corresponded to the Pt-S stretching mode ($\nu_{Pt\text{-}S}$), proving coordination of CDDP by thiol groups. The vibration band at 486 cm^{-1} attested the presence of silica (fourfold siloxane rings, $\nu(SiO_4)$, D1)[77,78]. For CDDP@MSNs-PEI, two new

bands appeared at 410 cm^{-1} and 598 cm^{-1}. Further data obtained with MSNs functionalized with amino groups and loaded with CDDP showed a vibration band at 396 cm^{-1} (data not shown), suggest formation of a complex between the primary amines of the amino groups and cisplatin. The broader band observed in the case of CDDP@MSNs-PEI may result from the different nature of the amines (primary, secondary and tertiary). However, the literature is lacking in this domain and more work is required to determine the composition of the complexes associated with these bands.

3.8 Preliminary study of CDDP release

To determine which of the surface-functionalized MSNs was the most appropriate in terms of CDDP release, preliminary release kinetics were performed using the well-known dynamic dialysis method[79]. Loaded MSNs were dispersed in 1 mM NaCl at a silica concentration of 4 mg/mL. Then, 2.5 mL of these suspensions were introduced in a dialysis bag (MWCO: 12 – 14 kDa). Platinum concentration outside the dialysis membrane was monitored over time by ICP-AES after the dialysis bag was immersed in 47.5 mL of RPMI 1640 culture medium

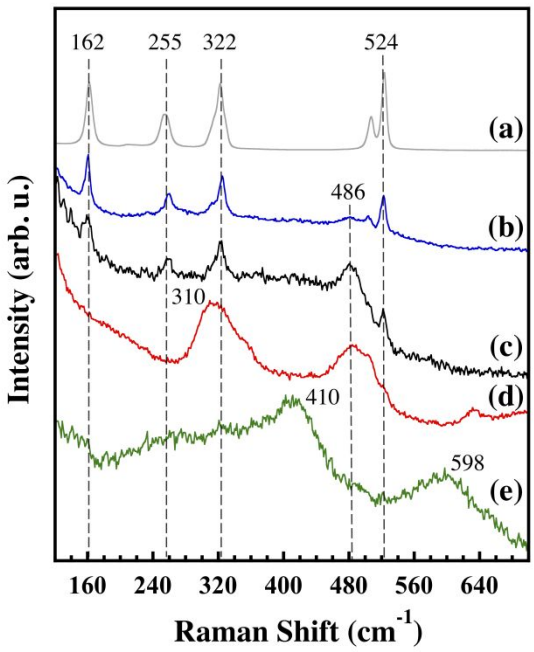

Figure 9: Raman spectra of (a) CDDP, (b) CDDP@MSNs-PEG, (c) CDDP@MSNs, (d) CDDP@MSNs-SH and (e) CDDP@MSNs-PEI.

incubated at 37°C (Fig. S7). As expected, the observation of a burst release was closely related to the homogeneity factor and followed this sequence after only 1 h of incubation: MSNs (29.3 %) > MSNs-PEG (23.1 %) > MSNs-PEI (2.5%) > MSNs-SH (0 %). As the homogeneity decreases, the burst release increases. This preliminary study also showed that despite no burst release was observed with CDDP@MSNs-SH, only 1.4 % of platinum-based species were released after 192 h of incubation, which confirm that platinum has a strong affinity for sulfur. However, the release of CDDP from this material could be triggered by the presence of biochemical thiols such as glutathione. Further studies are needed to confirm this hypothesis. On the opposite, a sustained release was observed for CDDP@MSNs, CDDP@MSNs-PEG and CDDP@MSNs-PEI with 53.8, 40.4 and 22.9 % of platinum-based species being released after 72 h of incubation, time for which the release process ended.

4. Conclusion

In this study, we have successfully synthesized MCM-41 silica nanoparticles functionalized either with (3-mercaptopropyl)triethoxysilane (MPTES) by co-condensation or with polyethylene glycol or low molecular weight branched polyethyleneimine using a postsynthesis grafting procedure. With a number of analytical tools, we have shown that the thiol groups were incorporated into the pores of the nanoparticles. Moreover, surface-modification with polymers allowed us to obtain monodispersed nanoparticles with a size of about 160 nm, with high porosity and colloidal stability for several days in aqueous solutions, which make these hybrid MSNs suitable for drug delivery applications.

To the best of our knowledge, this is the first study to describe the spectroscopic properties and spatial distribution of CDDP once loaded into MSNs. Depending on the functional group, platinum-based species were either dispersed in the nanomaterials as nanocrystals or as uniformly distributed species. Interestingly, spectral signature of CDDP was lost once loaded into PEI or thiol-functionalized MSNs.

Finally, PEI-functionalization showed the most promising results in terms of drug release considering the absence of burst release and a sustained release over several days. Combined with the property of low molecular weight PEI to increase the delivery of anticancer drugs into cancer cells while presenting a low cytotoxicity profile, this study highlights the potential of PEI-functionalized MSNs for efficient and safe cancer therapy using cisplatin.

Supporting Information

High magnification TEM images, colloidal stability of MSNs-PEI and MSNs-PEG, BET isotherms, BJH pore distributions, XRD patterns and TGA measurements, single-pulse ^{29}Si MAS NMR spectra of MSNs-SH, MSNs-COOH and pristine MSNs, Raman spectra of MSNs-SH and CDDP release profiles.

Acknowledgments

This study was supported by the Conseil Régional de Bourgogne under Contract No. 9201AAO03S05201 and by the 3MIM agreement (CNRS, UB and Conseil Régional de Bourgogne). We acknowledge Drs F. Herbst and N. Geoffroy for their advices in SEM and XRD characterizations, respectively. We also thank Dr Philippe Gaveau for solid state NMR spectroscopy.

Conflict of interests

The authors declare no conflict of interest.

References

(1) Ali, I.; Wani, W. A.; Saleem, K.; Haque, A. Platinum Compounds: A Hope for Future Cancer Chemotherapy. *Anticancer Agents Med. Chem.* **2013**, *13* (2), 296–306.
(2) Wheate, N. J.; Walker, S.; Craig, G. E.; Oun, R. The Status of Platinum Anticancer Drugs in the Clinic and in Clinical Trials. *Dalton Trans.* **2010**, *39* (35), 8113–8127. https://doi.org/10.1039/C0DT00292E.
(3) Rosenberg, B.; Vancamp, L.; Trosko, J. E.; Mansour, V. H. Platinum Compounds: A New Class of Potent Antitumour Agents. *Nature* **1969**, *222* (5191), 385–386. https://doi.org/10.1038/222385a0.
(4) Dugbartey, G. J.; Peppone, L. J.; de Graaf, I. A. M. An Integrative View of Cisplatin-Induced Renal and Cardiac Toxicities: Molecular Mechanisms, Current Treatment Challenges and Potential Protective Measures. *Toxicology* **2016**, *371*, 58–66. https://doi.org/10.1016/j.tox.2016.10.001.
(5) Lazarević, T.; Rilak, A.; Bugarčić, Ž. D. Platinum, Palladium, Gold and Ruthenium Complexes as Anticancer Agents: Current Clinical Uses, Cytotoxicity Studies and Future Perspectives. *Eur. J. Med. Chem.* **2017**, *142*, 8–31. https://doi.org/10.1016/j.ejmech.2017.04.007.
(6) Murakami, M.; Cabral, H.; Matsumoto, Y.; Wu, S.; Kano, M. R.; Yamori, T.; Nishiyama, N.; Kataoka, K. Improving Drug Potency and Efficacy by Nanocarrier-Mediated Subcellular Targeting. *Sci. Transl. Med.* **2011**, *3* (64), 64ra2. https://doi.org/10.1126/scitranslmed.3001385.
(7) Stathopoulos, G. P.; Boulikas, T. Lipoplatin Formulation Review Article. *J. Drug Deliv.* **2012**, *Volume 2012*, 10 pages.
(8) Paraskar, A.; Soni, S.; Roy, B.; Papa, A.-L.; Sengupta, S. Rationally Designed Oxaliplatin-Nanoparticle for Enhanced Antitumor Efficacy. *Nanotechnology* **2012**, *23* (7), 075103. https://doi.org/10.1088/0957-4484/23/7/075103.
(9) Ma, P.; Xiao, H.; Li, C.; Dai, Y.; Cheng, Z.; Hou, Z.; Lin, J. Inorganic Nanocarriers for Platinum Drug Delivery. *Mater. Today* **2015**, *18* (10), 554–564. https://doi.org/10.1016/j.mattod.2015.05.017.
(10) Min, Y.; Mao, C.-Q.; Chen, S.; Ma, G.; Wang, J.; Liu, Y. Combating the Drug Resistance of Cisplatin Using a Platinum Prodrug Based Delivery System. *Angew. Chem. Int. Ed.* **2012**, *51* (27), 6742–6747. https://doi.org/10.1002/anie.201201562.
(11) Cheng, Z.; Dai, Y.; Kang, X.; Li, C.; Huang, S.; Lian, H.; Hou, Z.; Ma, P.; Lin, J. Gelatin-Encapsulated Iron Oxide Nanoparticles for Platinum (IV) Prodrug Delivery, Enzyme-Stimulated Release and MRI. *Biomaterials* **2014**, *35* (24), 6359–6368. https://doi.org/10.1016/j.biomaterials.2014.04.029.
(12) Isaac, K. M.; Sabaraya, I. V.; Ghousifam, N.; Das, D.; Pekkanen, A. M.; Romanovicz, D. K.; Long, T. E.; Saleh, N. B.; Rylander, M. N. Functionalization of Single-Walled Carbon Nanohorns for Simultaneous Fluorescence Imaging and Cisplatin Delivery in Vitro. *Carbon* **2018**, *138*, 309–318. https://doi.org/10.1016/j.carbon.2018.06.020.
(13) Alvarez-Berríos, M. P.; Sosa-Cintron, N.; Rodriguez-Lugo, M.; Juneja, R.; Vivero-Escoto, J. L. Hybrid Nanomaterials Based on Iron Oxide Nanoparticles and Mesoporous Silica Nanoparticles: Overcoming Challenges in Current Cancer Treatments https://www.hindawi.com/journals/jchem/2016/2672740/ (accessed May 17, 2019). https://doi.org/10.1155/2016/2672740.
(14) Dréau, D.; Moore, L. J.; Alvarez-Berrios, M. P.; Tarannum, M.; Mukherjee, P.; Vivero-Escoto, J. L. Mucin-1-Antibody-Conjugated Mesoporous Silica Nanoparticles for Selective Breast Cancer Detection in a Mucin-1 Transgenic Murine Mouse Model. *J. Biomed.*

Nanotechnol. **2016**, *12* (12), 2172–2184. https://doi.org/10.1166/jbn.2016.2318.
(15) Vivero-Escoto, J. L.; Slowing, I. I.; Trewyn, B. G.; Lin, V. S.-Y. Mesoporous Silica Nanoparticles for Intracellular Controlled Drug Delivery. *Small* **2010**, *6* (18), 1952–1967. https://doi.org/10.1002/smll.200901789.
(16) Huh, S.; Wiench, J. W.; Yoo, J.-C.; Pruski, M.; Lin, V. S.-Y. Organic Functionalization and Morphology Control of Mesoporous Silicas via a Co-Condensation Synthesis Method. *Chem. Mater.* **2003**, *15* (22), 4247–4256. https://doi.org/10.1021/cm0210041.
(17) Cauda, V.; Argyo, C.; Schlossbauer, A.; Bein, T. Controlling the Delivery Kinetics from Colloidal Mesoporous Silica Nanoparticles with PH-Sensitive Gates. *J. Mater. Chem.* **2010**, *20* (21), 4305–4311. https://doi.org/10.1039/B918590A.
(18) Gary-Bobo, M.; Hocine, O.; Brevet, D.; Maynadier, M.; Raehm, L.; Richeter, S.; Charasson, V.; Loock, B.; Morère, A.; Maillard, P.; et al. Cancer Therapy Improvement with Mesoporous Silica Nanoparticles Combining Targeting, Drug Delivery and PDT. *Int. J. Pharm.* **2012**, *423* (2), 509–515. https://doi.org/10.1016/j.ijpharm.2011.11.045.
(19) Rosenholm, J. M.; Sahlgren, C.; Linden, M. Towards Multifunctional, Targeted Drug Delivery Systems Using Mesoporous Silica Nanoparticles - Opportunities & Challenges. *Nanoscale* **2010**, *2* (10), 1870–1883.
(20) Colilla, M.; Vallet-Regí, M. 4.35 Ordered Mesoporous Silica Materials. In *Comprehensive Biomaterials II*; Ducheyne, P., Ed.; Elsevier: Oxford, 2017; pp 644–685. https://doi.org/10.1016/B978-0-12-803581-8.10231-0.
(21) He, Q.; Zhang, J.; Shi, J.; Zhu, Z.; Zhang, L.; Bu, W.; Guo, L.; Chen, Y. The Effect of PEGylation of Mesoporous Silica Nanoparticles on Nonspecific Binding of Serum Proteins and Cellular Responses. *Biomaterials* **2010**, *31* (6), 1085–1092. https://doi.org/DOI: 10.1016/j.biomaterials.2009.10.046.
(22) Walker, W. A.; Tarannum, M.; Vivero-Escoto, J. L. Cellular Endocytosis and Trafficking of Cholera Toxin B-Modified Mesoporous Silica Nanoparticles. *J. Mater. Chem. B* **2016**, *4* (7), 1254–1262. https://doi.org/10.1039/C5TB02079D.
(23) Cauda, V.; Argyo, C.; Bein, T. Impact of Different PEGylation Patterns on the Long-Term Bio-Stability of Colloidal Mesoporous Silica Nanoparticles. *J. Mater. Chem.* **2010**, *20* (39), 8693–8699. https://doi.org/10.1039/C0JM01390K.
(24) Rosenholm, J. M.; Meinander, A.; Peuhu, E.; Niemi, R.; Eriksson, J. E.; Sahlgren, C.; Lindén, M. Targeting of Porous Hybrid Silica Nanoparticles to Cancer Cells. *ACS Nano* **2009**, *3* (1), 197–206. https://doi.org/10.1021/nn800781r.
(25) Cebriàn, V.; Yagüe, C.; Arruebo, M.; Martín-Saavedra, F.; Santamaría, J.; Vilaboa, N. On the Role of the Colloidal Stability of Mesoporous Silica Nanoparticles as Gene Delivery Vectors. *J. Nanoparticle Res.* **2011**, *13* (9), 4097–4108.
(26) Clemens, D. L.; Lee, B.-Y.; Xue, M.; Thomas, C. R.; Meng, H.; Ferris, D.; Nel, A. E.; Zink, J. I.; Horwitz, M. A. Targeted Intracellular Delivery of Antituberculosis Drugs to Mycobacterium Tuberculosis-Infected Macrophages via Functionalized Mesoporous Silica Nanoparticles. *Antimicrob Agents Chemother* **2012**, *56* (5), 2535–2545. https://doi.org/10.1128/AAC.06049-11.
(27) Neuberg, P.; Kichler, A. Chapter Nine - Recent Developments in Nucleic Acid Delivery with Polyethylenimines. In *Advances in Genetics*; Huang, L., Liu, D., Wagner, E., Eds.; Nonviral Vectors for Gene Therapy; Academic Press, 2014; Vol. 88, pp 263–288. https://doi.org/10.1016/B978-0-12-800148-6.00009-2.
(28) Rackley, L.; Stewart, J. M.; Salotti, J.; Krokhotin, A.; Shah, A.; Halman, J. R.; Juneja, R.; Smollett, J.; Lee, L.; Roark, K.; et al. RNA Fibers as Optimized Nanoscaffolds for SiRNA Coordination and Reduced Immunological Recognition. *Adv. Funct. Mater.* **2018**, *28* (48), 1805959. https://doi.org/10.1002/adfm.201805959.

(29) Xia, T.; Kovochich, M.; Liong, M.; Meng, H.; Kabehie, S.; George, S.; Zink, J. I.; Nel, A. E. Polyethyleneimine Coating Enhances the Cellular Uptake of Mesoporous Silica Nanoparticles and Allows Safe Delivery of SiRNA and DNA Constructs. *ACS Nano* **2009**, *3* (10), 3273–3286. https://doi.org/10.1021/nn900918w.
(30) Sun, X.; Chen, J.; Gu, X.; Liang, W.; Wang, J. Efficacy and Toxicity of Cisplatin Liposomes Modified with Polyethylenimine. *Pharm.* **2014**, *69* (4), 281–286.
(31) Gu, J.; Su, S.; Li, Y.; He, Q.; Zhong, J.; Shi, J. Surface Modification-Complexation Strategy for Cisplatin Loading in Mesoporous Nanoparticles. *J. Phys. Chem. Lett.* **2010**, *1* (24), 3446–3450. https://doi.org/10.1021/jz101483u.
(32) Gu, J.; Liu, J.; Li, Y.; Zhao, W.; Shi, J. One-Pot Synthesis of Mesoporous Silica Nanocarriers with Tunable Particle Sizes and Pendent Carboxylic Groups for Cisplatin Delivery. *Langmuir* **2013**, *29* (1), 403–410. https://doi.org/10.1021/la3036264.
(33) Lin, C.-H.; Cheng, S.-H.; Liao, W.-N.; Wei, P.-R.; Sung, P.-J.; Weng, C.-F.; Lee, C.-H. Mesoporous Silica Nanoparticles for the Improved Anticancer Efficacy of Cis-Platin. *Int. J. Pharm.* **2012**, *429* (1–2), 138–147. https://doi.org/10.1016/j.ijpharm.2012.03.026.
(34) Arean, C. O.; Vesga, M. J.; Parra, J. B.; Delgado, M. R. Effect of Amine and Carboxyl Functionalization of Sub-Micrometric MCM-41 Spheres on Controlled Release of Cisplatin. *Ceram. Int.* **2013**, *39* (7), 7407–7414. https://doi.org/10.1016/j.ceramint.2013.02.084.
(35) Alvarez-Berríos, M. P.; Vivero-Escoto, J. L. In Vitro Evaluation of Folic Acid-Conjugated Redox-Responsive Mesoporous Silica Nanoparticles for the Delivery of Cisplatin. *Int. J. Nanomedicine* **2016**, *11*, 6251–6265. https://doi.org/10.2147/IJN.S118196.
(36) Huang, L.; Liu, M.; Mao, L.; Huang, Q.; Huang, H.; Zeng, G.; Tian, J.; Wen, Y.; Zhang, X.; Wei, Y. A Facile FeBr3 Based PhotoATRP for Surface Modification of Mesoporous Silica Nanoparticles for Controlled Delivery Cisplatin. *Appl. Surf. Sci.* **2018**, *434*, 204–210. https://doi.org/10.1016/j.apsusc.2017.10.187.
(37) Hall, M. D.; Telma, K. A.; Chang, K.-E.; Lee, T. D.; Madigan, J. P.; Lloyd, J. R.; Goldlust, I. S.; Hoeschele, J. D.; Gottesman, M. M. Say No to DMSO: Dimethylsulfoxide Inactivates Cisplatin, Carboplatin, and Other Platinum Complexes. *Cancer Res.* **2014**, *74* (14), 3913–3922. https://doi.org/10.1158/0008-5472.CAN-14-0247.
(38) Fireman-Shoresh, S.; Hüsing, N.; Avnir, D. Adsorption/Desorption Characteristics of Cis-Platin on Mercapto-Silylated Silica Surfaces. *Langmuir* **2001**, *17* (19), 5958–5963. https://doi.org/10.1021/la010513z.
(39) Compañy, A. D.; Brizuela, G.; Simonetti, S. Effect of Thiol-Functionalised Silica on Cisplatin Adsorption. *Mol. Simul.* **2012**, *38* (13), 1055–1060. https://doi.org/10.1080/08927022.2012.690875.
(40) Varache, M.; Bezverkhyy, I.; Saviot, L.; Bouyer, F.; Baras, F.; Bouyer, F. Optimization of MCM-41 Type Silica Nanoparticles for Biological Applications: Control of Size and Absence of Aggregation and Cell Cytotoxicity. *J. Non-Cryst. Solids* **2015**, *408* (Supplement C), 87–97. https://doi.org/10.1016/j.jnoncrysol.2014.10.020.
(41) Varache, M.; Bezverkhyy, I.; Bouyer, F.; Chassagnon, R.; Baras, F.; Bouyer, F. Improving Structural Stability of Water-Dispersed MCM-41 Silica Nanoparticles through Post-Synthesis PH Aging Process. *J. Nanoparticle Res.* **2015**, *17* (9), 356. https://doi.org/10.1007/s11051-015-3147-6.
(42) Lang, N.; Tuel, A. A Fast and Efficient Ion-Exchange Procedure To Remove Surfactant Molecules from MCM-41 Materials. *Chem. Mater.* **2004**, *16* (10), 1961–1966. https://doi.org/10.1021/cm030633n.
(43) Walcarius, A.; Etienne, M.; Lebeau, B. Rate of Access to the Binding Sites in Organically Modified Silicates. 2. Ordered Mesoporous Silicas Grafted with Amine or Thiol Groups. *Chem. Mater.* **2003**, *15* (11), 2161–2173. https://doi.org/10.1021/cm021310e.

(44) Manzano, M.; Aina, V.; Areán, C. O.; Balas, F.; Cauda, V.; Colilla, M.; Delgado, M. R.; Vallet-Regí, M. Studies on MCM-41 Mesoporous Silica for Drug Delivery: Effect of Particle Morphology and Amine Functionalization. *Chem. Eng. J.* **2008**, *137* (1), 30–37. https://doi.org/10.1016/j.cej.2007.07.078.
(45) Massiot, D.; Fayon, F.; Capron, M.; King, I.; Le Calvé, S.; Alonso, B.; Durand, J.-O.; Bujoli, B.; Gan, Z.; Hoatson, G. Modelling One- and Two-Dimensional Solid-State NMR Spectra. *Magn. Reson. Chem.* **2002**, *40* (1), 70–76. https://doi.org/10.1002/mrc.984.
(46) Berners-Price, S. J.; Ronconi, L.; Sadler, P. J. Insights into the Mechanism of Action of Platinum Anticancer Drugs from Multinuclear {NMR} Spectroscopy. *Prog. Nucl. Magn. Reson. Spectrosc.* **2006**, *49* (1), 65–98. http://dx.doi.org/10.1016/j.pnmrs.2006.05.002.
(47) Anilanmert, B.; Yalçin, G.; Ariöz, F.; Dölen, E. The Spectrometric Determination of Cisplatin in Urine, Using o-Phenylenediamine as Derivatizing Agent. *Anal. Lett.* **2001**, *34* (1), 113–123. https://doi.org/10.1081/AL-100002709.
(48) Nakajima, N.; Ikada, Y. Mechanism of Amide Formation by Carbodiimide for Bioconjugation in Aqueous Media. *Bioconjug. Chem.* **1995**, *6* (1), 123–130. https://doi.org/10.1021/bc00031a015.
(49) Paris, J.; Bernhard, Y.; Boudon, J.; Heintz, O.; Millot, N.; Decréau, R. A. Phthalocyanine–Titanate Nanotubes: A Promising Nanocarrier Detectable by Optical Imaging in the so-Called Imaging Window. *RSC Adv.* **2014**, *5* (9), 6315–6322. https://doi.org/10.1039/C4RA13988G.
(50) Möller, K.; Kobler, J.; Bein, T. Colloidal Suspensions of Mercapto-Functionalized Nanosized Mesoporous Silica. *J. Mater. Chem.* **2007**, *17* (7), 624–631. https://doi.org/10.1039/B611931J.
(51) Kobler, J.; Möller, K.; Bein, T. Colloidal Suspensions of Functionalized Mesoporous Silica Nanoparticles. *ACS Nano* **2008**, *2* (4), 791–799. https://doi.org/10.1021/nn700008s.
(52) Franks, G. V. Zeta Potentials and Yield Stresses of Silica Suspensions in Concentrated Monovalent Electrolytes: Isoelectric Point Shift and Additional Attraction. *J. Colloid Interface Sci.* **2002**, *249* (1), 44–51. http://dx.doi.org/10.1006/jcis.2002.8250.
(53) Avadiar, L.; Leong, Y.-K. Interactions of PEI (Polyethylenimine)-Silica Particles with Citric Acid in Dispersions. *Colloid Polym. Sci.* **2011**, *289* (3), 237–245.
(54) Papa, A.-L.; Boudon, J.; Bellat, V.; Loiseau, A.; Bisht, H.; Sallem, F.; Chassagnon, R.; Bérard, V.; Millot, N. Dispersion of Titanate Nanotubes for Nanomedicine: Comparison of PEI and PEG Nanohybrids. *Dalton Trans.* **2014**, *44* (2), 739–746. https://doi.org/10.1039/C4DT02552K.
(55) Tripp, C. P.; Hair, M. L. An Infrared Study of the Reaction of Octadecyltrichlorosilane with Silica. *Langmuir* **1992**, *8* (4), 1120–1126. https://doi.org/10.1021/la00040a018.
(56) Morrow, B. A.; McFarlan, A. J. Chemical Reactions at Silica Surfaces. *J. Non-Cryst. Solids* **1990**, *120* (1–3), 61–71. http://dx.doi.org/10.1016/0022-3093(90)90191-N.
(57) Barabanova, A. I.; Pryakhina, T. A.; Afanas'ev, E. S.; Zavin, B. G.; Vygodskii, Y. S.; Askadskii, A. A.; Philippova, O. E.; Khokhlov, A. R. Anhydride Modified Silica Nanoparticles: Preparation and Characterization. *Appl. Surf. Sci.* **2012**, *258* (7), 3168–3172. http://dx.doi.org/10.1016/j.apsusc.2011.11.057.
(58) Izquierdo-Barba, I.; Ruiz-González, L.; Doadrio, J. C.; González-Calbet, J. M.; Vallet-Regí, M. Tissue Regeneration: A New Property of Mesoporous Materials. *Solid State Sci.* **2005**, *7* (8), 983–989. http://dx.doi.org/10.1016/j.solidstatesciences.2005.04.003.
(59) Kassab, H.; Maksoud, M.; Aguado, S.; Pera-Titus, M.; Albela, B.; Bonneviot, L. Polyethylenimine Covalently Grafted on Mesostructured Porous Silica for CO2 Capture. *RSC Adv.* **2012**, *2* (6), 2508–2516. https://doi.org/10.1039/C2RA01007K.
(60) Bhattacharyya, S.; Wang, H.; Ducheyne, P. Polymer-Coated Mesoporous Silica

Nanoparticles for the Controlled Release of Macromolecules. *Acta Biomater.* **2012**, *8* (9), 3429–3435. https://doi.org/10.1016/j.actbio.2012.06.003.
(61) Hayashi, T.; Mukamel, S. Two-Dimensional Vibrational Lineshapes of Amide III, II, I and A Bands in a Helical Peptide. *J. Mol. Liq.* **2008**, *141* (3), 149–154. http://dx.doi.org/10.1016/j.molliq.2008.02.013.
(62) Dong, Y.; Wang, R.; Li, H.; Shao, J.; Chi, Y.; Lin, X.; Chen, G. Polyamine-Functionalized Carbon Quantum Dots for Chemical Sensing. *Carbon* **2012**, *50* (8), 2810–2815. http://dx.doi.org/10.1016/j.carbon.2012.02.046.
(63) Sadasivan, S.; Khushalani, D.; Mann, S. Synthesis and Shape Modification of Organo-Functionalised Silica Nanoparticles with Ordered Mesostructured Interiors. *J. Mater. Chem.* **2003**, *13* (5), 1023–1029. https://doi.org/10.1039/B300851G.
(64) Du, X.; He, J. Elaborate Control over the Morphology and Structure of Mercapto-Functionalized Mesoporous Silicas as Multipurpose Carriers. *Dalton Trans* **2010**, *39* (38), 9063–9072. https://doi.org/10.1039/C0DT00194E.
(65) Chen, M.-L.; Zhang, J.; Zhang, Z.; Yuan, B.-F.; Yu, Q.-W.; Feng, Y.-Q. Facile Preparation of Organic-Silica Hybrid Monolith for Capillary Hydrophilic Liquid Chromatography Based on "Thiol-Ene" Click Chemistry. *J. Chromatogr. A* **2013**, *1284*, 118–125. https://doi.org/10.1016/j.chroma.2013.02.008.
(66) Lee, C. H.; Park, S. H.; Chung, W.; Kim, J. Y.; Kim, S. H. Preparation and Characterization of Surface Modified Silica Nanoparticles with Organo-Silane Compounds. *Colloids Surf. Physicochem. Eng. Asp.* **2011**, *384* (1–3), 318–322. http://dx.doi.org/10.1016/j.colsurfa.2011.04.010.
(67) Zhang, Y.; Xu, Q.; Zhang, S.; Liu, J.; Zhou, J.; Xu, H.; Xiao, H.; Li, J. Preparation of Thiol-Modified Fe3O4@SiO2 Nanoparticles and Their Application for Gold Recovery from Dilute Solution. *Sep. Purif. Technol.* **2013**, *116* (0), 391–397. http://dx.doi.org/10.1016/j.seppur.2013.06.018.
(68) Bosch, M. E.; Sánchez, A. J. R.; Rojas, F. S.; Ojeda, C. B. Analytical Methodologies for the Determination of Cisplatin. *J. Pharm. Biomed. Anal.* **2008**, *47* (3), 451–459. https://doi.org/10.1016/j.jpba.2008.01.047.
(69) Golla, E. D.; Ayres, G. H. Spectrophotometric Determination of Platinum with O-Phenylenediamine. *Talanta* **1973**, *20* (2), 199–210. http://dx.doi.org/10.1016/0039-9140(73)80267-X.
(70) Shabir, G. A.; Lough, W. J.; Arain, S. A.; Bradshaw, T. K. Evaluation and Application of Best Practice in Analytical Method Validation. *J. Liq. Chromatogr. Relat. Technol.* **2007**, *30* (3), 311–333. https://doi.org/10.1080/10826070601084753.
(71) Riley, C. M.; Sternson, L. A. Cisplatin. In *Analytical Profiles of Drug Substances*; Florey, K., Ed.; Academic Press, 1985; Vol. 14, pp 77–105.
(72) Dabrowiak, J. C.; Goodisman, J.; Souid, A.-K. Kinetic Study of the Reaction of Cisplatin with Thiols. *Drug Metab. Dispos.* **2002**, *30* (12), 1378–1384. https://doi.org/10.1124/dmd.30.12.1378.
(73) Baik, M.-H.; Friesner, R. A.; Lippard, S. J. Theoretical Study of Cisplatin Binding to Purine Bases: Why Does Cisplatin Prefer Guanine over Adenine? *J. Am. Chem. Soc.* **2003**, *125* (46), 14082–14092. https://doi.org/10.1021/ja036960d.
(74) Vivero-Escoto, J. L.; Elnagheeb, M. Mesoporous Silica Nanoparticles Loaded with Cisplatin and Phthalocyanine for Combination Chemotherapy and Photodynamic Therapy in Vitro. *Nanomater. Basel Switz.* **2015**, *5* (4), 2302–2316. https://doi.org/10.3390/nano5042302.
(75) Amado, A. M.; Fiuza, S. M.; Marques, M. P. M.; Carvalho, L. A. E. B. de. Conformational and Vibrational Study of Platinum(II) Anticancer Drugs: Cis-Diamminedichloroplatinum (II) as a Case Study. *J. Chem. Phys.* **2007**, *127* (18), 185104.

https://doi.org/10.1063/1.2787528.
(76) Torres, M.; Khan, S.; Duplanty, M.; Lozano, H. C.; Morris, T. J.; Nguyen, T.; Rostovtsev, Y. V.; DeYonker, N. J.; Mirsaleh-Kohan, N. Raman and Infrared Studies of Platinum-Based Drugs: Cisplatin, Carboplatin, Oxaliplatin, Nedaplatin, and Heptaplatin. *J. Phys. Chem. A* **2018**, *122* (34), 6934–6952. https://doi.org/10.1021/acs.jpca.8b04023.
(77) Chao, K. J.; Wu, C. N.; Chang, H.; Lee, L. J.; Hu, S. Incorporation of Vanadium in Mesoporous MCM-41 and Microporous AFI Zeolites. *J. Phys. Chem. B* **1997**, *101* (33), 6341–6349. https://doi.org/10.1021/jp970609v.
(78) Brinker, C. J.; Kirkpatrick, R. J.; Tallant, D. R.; Bunker, B. C.; Montez, B. NMR Confirmation of Strained "Defects" in Amorphous Silica. *J. Non-Cryst. Solids* **1988**, *99* (2–3), 418–428. https://doi.org/10.1016/0022-3093(88)90448-6.
(79) Modi, S.; Anderson, B. D. Determination of Drug Release Kinetics from Nanoparticles: Overcoming Pitfalls of the Dynamic Dialysis Method. *Mol. Pharm.* **2013**, *10* (8), 3076–3089. https://doi.org/10.1021/mp400154a.

Table of Contents/Graphical Abstract